PHYSICAL REVIEW B **80**, 180417(R) (2009)

Competing interactions in ferromagnetic/antiferromagnetic perovskite superlattices

Y. Takamura,[1] F. Yang,[1] N. Kemik,[1] E. Arenholz,[2] M. D. Biegalski,[3] and H. M. Christen[3]
[1]*Department of Chemical Engineering and Materials Science, University of California–Davis, Davis, California 95616, USA*
[2]*Advanced Light Source, Lawrence Berkeley National Laboratory, Berkeley, California 94720, USA*
[3]*Center for Nanophase Materials Science, Oak Ridge National Laboratory, Oak Ridge, Tennessee 37831, USA*
(Received 22 October 2009; published 19 November 2009)

Soft x-ray magnetic dichroism, magnetization, and magnetotransport measurements demonstrate that the competition between different magnetic interactions (exchange coupling, electronic reconstruction, and long-range interactions) in $La_{0.7}Sr_{0.3}FeO_3$(LSFO)/$La_{0.7}Sr_{0.3}MnO_3$(LSMO) perovskite oxide superlattices leads to unexpected functional properties. The antiferromagnetic order parameter in LSFO and ferromagnetic order parameter in LSMO show a dissimilar dependence on sublayer thickness and temperature, illustrating the high degree of tunability in these artificially layered materials.

DOI: 10.1103/PhysRevB.80.180417 PACS number(s): 75.70.Cn, 75.47.Gk, 78.70.Dm

Complex materials with multiple order parameters hold the promise to yield multiferroic systems with highly tunable and stimulus-sensitive properties as required for sensing, energy conversion, and information technology applications.[1] Specifically, the class of perovskite oxides (ABO_3) has garnered much attention due to the possibility of creating epitaxial superlattices composed of stacks of alternating sublayers, each with their own order parameter, formed with atomic-scale control, and designed to exploit interactions at and across interfaces.[2–6] However, the competition between multiple order parameters places a great challenge on our ability to predict the resulting physical properties and thus to create complex materials which meet specific application requirements. A few remarkable examples have shown the appearance of an additional order parameter (i.e., superconductivity or ferromagnetism) at interfaces despite the fact that it does not exist in the constituent materials.[6–8] Exchange bias interactions occur at interfaces between antiferromagnetic (AF) and ferromagnetic (FM) layers and they have commonly been utilized in metallic systems to pin the magnetization of the reference electrode in magnetic recording read heads. However, the spins within the surface layer of a *G*-type AF such as $La_{1-x}Sr_xFeO_3$ are compensated, and in this case exchange interactions are predicted to occur via the spin-flop mechanism such that the direction of the AF spin axis can be reoriented by an applied magnetic field.[9–11] We recently confirmed this prediction in an all-perovskite oxide superlattice consisting of alternating six-unit-cell-thick $La_{0.7}Sr_{0.3}MnO_3$ (LSMO) and $La_{0.7}Sr_{0.3}FeO_3$ (LSFO) layers.[12] In the present study, we show that the AF and FM properties in this superlattice system exhibit dissimilar dependencies on temperature and sublayer thickness and we identify the importance of short-range electronic effects (i.e., charge transfer), in addition to long-range (dipole) interactions and magnetic anisotropy. These results illustrate the importance of the delicate balance between exchange coupling, electronic reconstruction, and long-range interactions in these interfacial phenomena.

LSMO exhibits colossal magnetoresistance, a high degree of spin polarization, a Curie temperature above room temperature ($T_C \sim 360$ K),[13] as well as coincident FM/paramagnetic and metal/insulator transitions mediated by the Mn^{3+}/Mn^{4+} double exchange mechanism.[14] These properties make LSMO a promising electrode material for information technology applications. The replacement of Mn with Fe on the *B* site leads to an AF insulator state in LSFO with a Néel temperature, $T_N \sim 360$ K,[15,16] similar to the T_C of LSMO for the same Sr/La ratio. The uniform doping level across both layers prevents Sr diffusion between layers while the differing B site element allows us to independently probe the AF and FM properties using x-ray absorption (XA) spectroscopy by tuning to the Fe and Mn absorption edges, respectively. Therefore, this system represents an ideal model system for investigating the interfacial coupling between FM and AF perovskite layers.

LSMO and LSFO epitaxial films and superlattices were grown on (001)-oriented single-crystal $SrTiO_3$(STO) substrates by pulsed laser deposition using a KrF laser (248 nm) at 10 Hz, a fluence ~ 1.2 J/cm^2, a substrate temperature of 700 °C and an oxygen pressure of 200 mTorr. *In situ* reflection high energy electron diffraction monitored the growth rate and verified the layer-by-layer growth mode. After deposition, the superlattices were cooled slowly to room temperature in an oxygen pressure of ~300 Torr to ensure the proper oxygenation of the films. The notation for the superlattices consists of the following: [*number unit cells LSFO* × *number unit cells LSMO*] *number of repeats*. In all cases, an equal number of LSMO and LSFO unit cells were grown; the LSMO layer was grown first, so that the LSFO layer lies at the surface of the superlattice. For comparison, single layer films with ~40 nm thickness of LSMO, LSFO, and the LSFO/LSMO solid solution (i.e., $La_{0.7}Sr_{0.3}Fe_{0.5}Mn_{0.5}O_3$) were also grown.

Atomic force microscopy shows an exceptionally low rms roughness below 0.5 nm, irrespective of the superlattice period. The structural properties of the films were measured by x-ray reflectivity and high-resolution x-ray diffraction (XRD) using a Bruker D8 Discover four-circle diffraction system and beamlines 2–1 and 7–2 at the Stanford Synchrotron Radiation Laboratory (SSRL). Satellite peaks and thickness fringes are observed for the superlattices in the *l* scans of the out-of-plane 002 reflection, attesting to the smooth interfaces and permitting us to accurately confirm the periodicity of the superlattice structures. Reciprocal space maps around the 103, 301, and 331 reflections demonstrate that all superlattices are fully strained to the STO substrate. Therefore, in thin-film form we can describe rhombohedral LSMO and orthorhombic LSFO using their pseudotetragonal lattice so

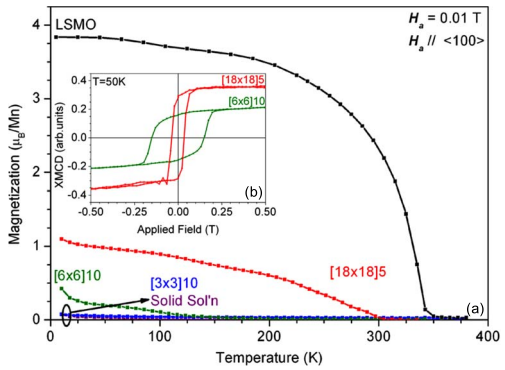

FIG. 1. (Color online) (a) Magnetization as a function of temperature for the superlattices, solid solution film, and LSMO film with H_a=0.01 T, and (b) XMCD hysteresis loops for $[6\times6]10$ and $[18\times18]5$ at 50 K. The magnitude of XMCD difference reflects a correction for the differing background ratio for each sample.

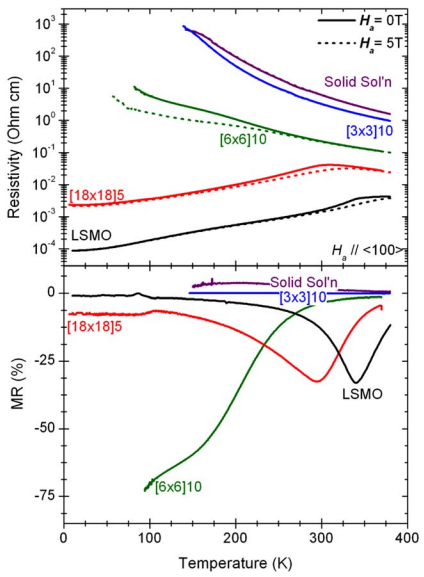

FIG. 2. (Color online) (a) Resistivity and (b) magnetoresistance, $MR=[\rho(H=5T)-\rho(H=0T)]/\rho(H=0T)\times100$ as a function of temperature for the superlattices, solid solution film, and LSMO film.

that the films share the same crystallographic indices as the cubic STO substrate ($a=b\neq c$, with c normal to the substrate surface). The LSMO and LSFO layers undergo the same tetragonal distortion independent of the sublayer thickness. The full widths at half maximum (FWHM) of the film ω scans for the superlattices (0.024–0.028°) and the solid solution (0.039°) were only slightly higher than the typical value of ~0.013° for the substrate, again confirming the high degree of crystallinity.

The macroscopic magnetization was measured using a Quantum Design superconducting quantum interference device (SQUID) magnetometer, with the magnetic field applied in the plane of the film either along the ⟨100⟩ or ⟨110⟩ substrate directions. The temperature dependence (Fig. 1) was measured for the LSMO film, superlattices, and solid solution film with an applied magnetic field, H_a=0.01 T. The magnetization is normalized to the thickness of the LSMO layers only. The LSMO film exhibits bulklike $T_c\sim340$ K and saturation magnetization, $M_s\sim3.8\mu_B$/Mn at 10 K. No appreciable magnetization is observed for the solid solution film in agreement with results for Fe-doped manganites.[17,18] With decreasing sublayer thickness, the values of T_C and M_s decrease, reaching 300 and ~150–200 K, and $1.47\mu_B$/Mn and $0.57\mu_B$/Mn for $[18\times18]5$ and $[6\times6]10$, respectively. Finally, the magnetization of $[3\times3]10$ approaches that of the solid solution film. This trend of reduced T_C and M_s agrees with reports for ultrathin LSMO films below ~20 unit cells.[19–23] Hysteresis loops show that the easy magnetization direction for all superlattices lies along the ⟨110⟩ direction, in agreement with published results for LSMO films grown on (001)-oriented STO substrates as a consequence of the 0.64% tensile strain imposed from the substrate.[24] The coercive field for $[18\times18]5$ at 10 K is ~0.048 T, only slightly higher than that of an LSMO film on STO. However, the coercive field increases to ~0.17 T for $[6\times6]10$, indicating that the magnetization reversal in the LSMO layer is influenced by the exchange coupling to the adjacent LSFO layer at small sublayer thicknesses, as discussed below.

Magnetotransport properties as a function of temperature (Fig. 2) were measured using the van der Pauw geometry with H_a=0 and 5 T applied along the in-plane ⟨100⟩ direction. The resistivity, ρ, of each superlattice is calculated from its resistance using the simplified assumption that the entire stack rather than only the lower-resistivity LSMO layers contribute to the conduction. Mirroring the magnetization data, the superlattices' $\rho(T)$ behavior approaches that of the solid solution film with decreasing period. A well-defined metal-insulator transition at T_C is observed only in the LSMO film and the $[18\times18]5$ superlattice and it is accompanied by a negative peak in the magnetoresistance, $MR=[\rho(H=5T)-\rho(H=0T)]/\rho(H=0T)\times100$. While already in $[18\times18]5$, the T_C is depressed by 40 K and the resistivity increased by an order of magnitude across the entire temperature range, the behavior of these thicker LSMO sublayers differs fundamentally from that of the $[3\times3]10$ superlattice and solid solution film. These samples display insulating behavior across the entire temperature range, no significant magnetization, and thus no MR. At intermediate period, $[6\times6]10$ exhibits insulating characteristics with a large negative MR which monotonically increases in magnitude with decreasing temperature. A similar MR behavior has been reported in ultrathin (approximately four unit cells) LSMO films[22] as well as LSMO films under large tensile strain,[25] though it may also be related to the exchange coupling between the adjacent LSFO and LSMO layers.

X-ray magnetic circular and linear dichroism (XMCD/XMLD) experiments were performed at beamlines 4.0.2 and 6.3.1 of the Advanced Light Source[26] in order to probe the near surface FM/AF properties of the superlattices with element specificity. XMCD spectra were obtained at 30° grazing incidence with H_a=+/−0.27 T parallel to the x-ray beam. The Mn XMCD data [Fig. 1(b)] exhibit the same sublayer thickness dependence as the SQUID data, i.e., a decreasing magnetization with decreasing sublayer thickness. This result demonstrates the magnetic uniformity of the superlattice stacks, allowing us to conclude that near surface XA data is representative of the entire superlattice and that

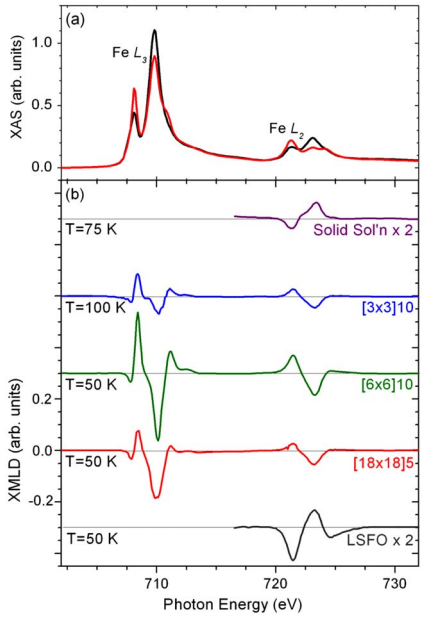

FIG. 3. (Color online) (a) XA spectra for the $[6\times6]10$ superlattice with $\boldsymbol{E}\|[001]$ (black curve) and $\boldsymbol{E}\|[010]$ (red/gray curve), and (b) XMLD spectra defined as $\boldsymbol{E}\|[010]-\boldsymbol{E}\|[001]$ for the superlattices, solid solution film, and LSFO film. All superlattices possess the same characteristics which are *opposite* to that of the solid solution and LSFO films. Due to experimental artifacts with insulating films, only the Fe L_2 edge is shown for the single layer films.

any difference in sample thickness does not contribute to the observed trends.

In bulk LSFO the AF spin axis, $\boldsymbol{M}_{\mathrm{Fe}}$, lies along the crystallographic $\boldsymbol{a}$ axis[27] while studies of $LaFeO_3$ thin films[28,29] show that the direction of $\boldsymbol{M}_{\mathrm{Fe}}$ differs from the bulk and is sensitive to the growth method and strain state. Therefore, to analyze the direction of $\boldsymbol{M}_{\mathrm{Fe}}$ in our superlattices, we reference its orientation to that of our LSFO films. The AF order in the LSFO layers was probed through Fe $L_{3,2}$ XMLD spectra obtained in grazing incidence with $H_a=0$ and the x-rays impinging at 30° with respect to the sample surface. The x-ray polarization, $\boldsymbol{E}$, is applied either in-plane (along the [010] substrate direction) or at 60° with respect to the sample surface (referred to as the out-of-plane [001] substrate direction) and thereby providing information on the orientation of $\boldsymbol{M}_{\mathrm{Fe}}$ with respect to the sample surface.

For temperatures below 100 K, the Fe XMLD spectra (Fig. 3) for all superlattices are nearly identical whereas the sign of the XMLD is reversed for the solid solution and LSFO films. To interpret these spectra, we first note that the Fe^{3+} ions in LSFO are surrounded by O^{2-} ions in an octahedral symmetry, similar to that of the Fe^{3+} on the B site in the spinel Fe_3O_4. Therefore, we employ the analysis of XMLD spectra as described in Ref. 30, which indicates an in-plane alignment of $\boldsymbol{M}_{\mathrm{Fe}}$ in the superlattices and conversely an out-of-plane canting for the solid solution and LSFO films. This in-plane confinement is believed to occur due to the presence of a high density of interfaces and the 2D nature of the superlattice structures. A full determination of the direction of $\boldsymbol{M}_{\mathrm{Fe}}$ using photoemission electron microscopy will be discussed elsewhere.[31] These equally strained solid solution and

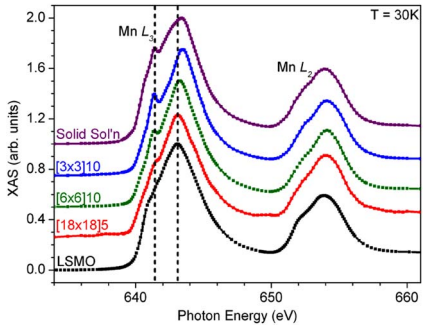

FIG. 4. (Color online) Mn XA spectra for the superlattices, solid solution film, and LSMO film. An additional feature 2 eV below the main Mn L_3 peak appears as the sublayer thickness decreases.

LSFO films are used as "end-member" reference points, allowing us to conclude that the AF properties of the superlattices do not approach those of the end members, contrary to the case of the FM behavior of the same superlattices. The AF signature remains in the LSFO film as well as $[6\times6]10$ and $[18\times18]5$ beyond room temperature but disappears for $[3\times3]10$ and the solid solution film between 150 K and room temperature. Even without a full investigation of the temperature dependence of T_N, we clearly observe a gradual trend of decreasing T_N with decreasing sublayer thickness. This decrease occurs much more slowly than the observed decrease in the T_C of the LSMO layers, such that even at three unit-cell thickness, the LSFO layer remains in an AF state. Comparatively fewer studies have been performed on the thickness dependence of AF properties, particularly for the perovskite oxides, though reports on NiO have shown a rapid decrease in T_N between five and ten unit cell film thickness.[32] Therefore, the AF properties in this superlattice structure exhibit a fundamentally different dependence on the sublayer thickness and between thin films and superlattices than their FM counterparts.

In order to further explore the differing thickness dependence of the FM and AF properties of the superlattices, the XA spectra for the Mn $L_{3,2}$ absorption edges of the samples are shown in Fig. 4. The solid solution film and $[3\times3]10$ display a slight shift of the main L_3 peak to higher photon energy as well as the presence of an additional peak about 2 eV below the main L_3 peak. These signatures have been ascribed to an increased concentration of Mn^{4+} ions.[33,34] Due to the uniform Sr doping level, the change in the Mn^{3+}/Mn^{4+} ratio is not expected to be related to A-site chemical doping effects. Alternatively, a charge transfer involving an electron transferring from the LSMO layers to LSFO layers ($Mn^{3+}\rightarrow Mn^{4+}$) across the interface as proposed by Kumigashira and co-workers[35] might be expected. The ground state of the LSFO system for small Sr doping ($x<0.5$) is the Fe^{3+}-ligand hole state.[33] In accordance, the electrons involved in the charge transfer go to states of primarily oxygen character and no significant difference is observed in the Fe XA spectra for any sample. Characteristic length scales over which such charge-transfer mechanisms occur have been determined in other perovskite systems, such as $SrTiO_3/LaTiO_3$ (Ref. 36) and $LaMnO_3/SrMnO_3$ (Ref. 37) and typically range in the order of a few unit cells, consistent with our observations. The interfacially induced valence

changes effectively push the LSMO system toward the case of *higher* Sr doping (yielding a FM metal with *decreased* T_C). Therefore, together with the decrease in long-range (dipole) interactions due to finite-size effects, this mechanism clearly contribute to the rapid decrease of T_C and M_s with decreasing sublayer thickness, i.e., the magnetization and magnetotransport properties trend from those of the LSMO film toward the solid solution film. For the LSFO sublayers, the Fe valence state is nearly unchanged by the charge transfer, and consequently the T_N is only weakly dependent on sublayer thickness. The observed gradual decrease in T_N is likely due to the decrease in magnetic anisotropy with decreasing sublayer thickness.[32] Additional effects (such as interfacial stabilization of oxygen vacancies within LSFO even in strong oxidizing conditions) cannot be ruled out. These results illustrate the complexity of the effects observed at interfaces and the importance of determining the properties on the length scale of a few unit cells.

An additional XMLD measurement allows us to investigate the coupling between the LSFO and LSMO layers in the superlattices. These measurements (discussed in detail elsewhere[12]) are taken in a normal-incidence geometry with H_a=0.3 T parallel or perpendicular to the x-ray $\boldsymbol{E}$ vector. This magnetic field is sufficient to align the Mn moments in any direction within the surface plane. Any coupling between the LSFO and LSMO layers will result in an observable change in the Fe $L_{3,2}$ XA spectra. The solid solution film and $[3\times3]10$ show no FM order and as expected, no coupling is observed. In contrast, for $[6\times6]10$ we find a robust orthogonal coupling between the LSFO and LSMO layers, imposing an orientation of $\boldsymbol{M}_{\mathrm{Fe}}$ such that it lies within the film plane but at 90° with respect to the in-plane Mn moments regardless of their direction within the plane. This result agrees with predictions from a microscopic Heisenberg model[9–11] for the (001)-surface of a *G*-type AF such as LSFO, where an equal number of positive and negative exchange interactions exist. The large coercive field observed in the magnetization data for this sample confirms the importance of the exchange coupling. Upon further increase in the sublayer thickness to $[18\times18]5$, the XMLD decreases to near zero: the magnetic anisotropy in the LSFO layers now dominates. Thus, exchange coupling at this thickness plays a comparatively weaker role, and the coercive field correspondingly returns to a value near that of the LSMO film.

In summary, we have characterized a series of all-perovskite oxide superlattice structures consisting of AF LSFO layers and FM LSMO layers: two materials which exhibit nearly equal critical temperatures in the bulk. The two order parameters display dissimilar behavior with decreasing temperature and sublayer thickness. For LSFO, 2D confinement and a high density of interfaces preserves an in-plane orientation of the AF axis and the magnetic anisotropy and T_N gradually decrease, while for LSMO, the FM properties trend toward the solid solution due to the combined effects of a charge transfer at the LSFO interfaces and diminished long-range interactions. For $[6\times6]10$, a balance exists between the exchange interactions, interfacial electronic reconstruction, and long-range interactions leading to a robust spin-flop coupling. For decreasing LSMO sublayer thickness, the ferromagnetism is lost, while for increasing LSFO sublayer thickness, the magnetic anisotropy of the LSFO layer dominates. Understanding the competition between these interactions provides a promising means to separately control the FM and AF properties in superlattice structures, independent of strain or chemical effects.

We thank A. Mehta and M. Bibee (SSRL) for assistance in acquiring the XRD data and R. Chopdekar and Y. Suzuki (UC Berkeley) for assistance with the magnetotransport measurements. Research at the ALS (Contract No. DE-AC02-05CH11231), CNMS, and SSRL is supported by the Division of Scientific User Facilities, Office of Basic Energy Sciences, U.S. Department of Energy. Research at UC Davis is supported by UC Davis start-up funds and the National Science Foundation (Contract No. DMR 0747896) (Y.T.).

[1] R. Ramesh and N. A. Spaldin, Nature Mater. **6**, 21 (2007).
[2] H. Yamada *et al.*, Science **305**, 646 (2004).
[3] D. G. Schlom *et al.*, J. Am. Ceram. Soc. **91**, 2429 (2008).
[4] H. N. Lee *et al.*, Nature (London) **433**, 395 (2005).
[5] H. M. Christen *et al.*, Appl. Phys. A: Mater. Sci. Process. **93**, 807 (2008).
[6] A. Ohtomo and H. Y. Hwang, Nature (London) **427**, 423 (2004).
[7] R. Pentcheva and W. E. Pickett, Phys. Rev. B **74**, 035112 (2006).
[8] N. Reyren *et al.*, Science **317**, 1196 (2007).
[9] L. L. Hinchey and D. L. Mills, Phys. Rev. B **34**, 1689 (1986).
[10] N. C. Koon, Phys. Rev. Lett. **78**, 4865 (1997).
[11] T. C. Schulthess and W. H. Butler, Phys. Rev. Lett. **81**, 4516 (1998).
[12] E. Arenholz *et al.*, Appl. Phys. Lett. **94**, 072503 (2009).
[13] A. P. Ramirez, J. Phys.: Condens. Matter **9**, 8171 (1997).
[14] P.-G. de Gennes, Phys. Rev. **118**, 141 (1960).
[15] J.-C. Grenier *et al.*, Mater. Res. Bull. **19**, 1301 (1984).
[16] U. Shimony and J. M. Knudsen, Phys. Rev. **144**, 361 (1966).
[17] K. H. Ahn *et al.*, Phys. Rev. B **54**, 15299 (1996).
[18] A. Tiwari and K. P. Rajeev, J. Appl. Phys. **86**, 5175 (1999).
[19] C. A. F. Vaz *et al.*, Rep. Prog. Phys. **71**, 056501 (2008).
[20] M. Huijben *et al.*, Phys. Rev. B **78**, 094413 (2008).
[21] R. V. Chopdekar *et al.*, Phys. Rev. B **79**, 104417 (2009).
[22] J. Z. Sun *et al.*, Appl. Phys. Lett. **74**, 3017 (1999).
[23] A. Tebano *et al.*, Phys. Rev. Lett. **100**, 137401 (2008).
[24] L. M. Berndt *et al.*, Appl. Phys. Lett. **77**, 2903 (2000).
[25] Y. Takamura *et al.*, Appl. Phys. Lett. **92**, 162504 (2008).
[26] E. Arenholz and S. O. Prestemon, Rev. Sci. Instrum. **76**, 083908 (2005).
[27] R. L. White, J. Appl. Phys. **40**, 1061 (1969).
[28] J. Luning *et al.*, Phys. Rev. B **67**, 214433 (2003).
[29] S. Czekaj *et al.*, Phys. Rev. B **73**, 020401(R) (2006).
[30] E. Arenholz *et al.*, Phys. Rev. B **74**, 094407 (2006).
[31] Y. Takamura (unpublished).
[32] D. Alders *et al.*, Phys. Rev. B **57**, 11623 (1998).
[33] M. Abbate *et al.*, Phys. Rev. B **46**, 4511 (1992).
[34] F. M. F. de Groot, J. Electron Spectrosc. Relat. Phenom. **67**, 529 (1994).
[35] H. Kumigashira *et al.*, Appl. Phys. Lett. **84**, 5353 (2004).
[36] A. Ohtomo *et al.*, Nature (London) **419**, 378 (2002).
[37] S. Smadici *et al.*, Phys. Rev. Lett. **99**, 196404 (2007).